

This article was published in an Elsevier journal. The attached copy is furnished to the author for non-commercial research and education use, including for instruction at the author's institution, sharing with colleagues and providing to institution administration.

Other uses, including reproduction and distribution, or selling or licensing copies, or posting to personal, institutional or third party websites are prohibited.

In most cases authors are permitted to post their version of the article (e.g. in Word or Tex form) to their personal website or institutional repository. Authors requiring further information regarding Elsevier's archiving and manuscript policies are encouraged to visit:

<http://www.elsevier.com/copyright>



ELSEVIER

Available online at [www.sciencedirect.com](http://www.sciencedirect.com)

Nuclear Instruments and Methods in Physics Research A 583 (2007) 372–381

**NUCLEAR  
INSTRUMENTS  
& METHODS  
IN PHYSICS  
RESEARCH**  
Section A

[www.elsevier.com/locate/nima](http://www.elsevier.com/locate/nima)

# High efficiency plastic scintillator detector with wavelength-shifting fiber readout for the GLAST Large Area Telescope

A.A. Moiseev<sup>a,\*</sup>, P.L. Deering<sup>b,1</sup>, R.C. Hartman<sup>c</sup>, T.E. Johnson<sup>c</sup>, T.R. Nebel<sup>b</sup>,  
J.F. Ormes<sup>d</sup>, D.J. Thompson<sup>c</sup>

<sup>a</sup>*CRESST and Astrophysics Science Division, NASA's Goddard Space Flight Center, Greenbelt, MD 20771, USA*

<sup>b</sup>*Fermi National Accelerator Laboratory, Batavia, IL 60510, USA*

<sup>c</sup>*NASA's Goddard Space Flight Center, Greenbelt, MD 20771, USA*

<sup>d</sup>*University of Denver, Denver, CO 80208, USA*

Received 20 September 2007; received in revised form 24 September 2007; accepted 24 September 2007

Available online 29 September 2007

## Abstract

This paper describes the design and performance studies of the scintillator tile detectors for the anti-coincidence detector (ACD) of the Large Area Telescope (LAT) on the Gamma ray Large Area Space Telescope (GLAST), scheduled for launch in early 2008. The scintillator tile detectors utilize wavelength-shifting fibers and have dual-photomultiplier-tube readout. The design requires highly efficient and uniform detection of singly charged relativistic particles over the tile area and must meet all requirements for a launch, as well as operation in a space environment. We present here the design of three basic types of tiles used in the ACD, ranging in size from  $\sim 450$  to  $\sim 2500 \text{ cm}^2$ , all  $\sim 1 \text{ cm}$  thick, with different shapes, and with photoelectron yield of  $\sim 20$  photoelectrons per minimum ionizing particle at normal tile incidence, uniform over the tile area. Some tiles require flexible clear fiber cables up to 1.5 m long to deliver scintillator light to remotely located photomultiplier tubes.

© 2007 Elsevier B.V. All rights reserved.

PACS: 07.87.+v; 95.55.Ka

Keywords: GLAST; ACD; Anti-coincidence; Plastic scintillator; WLS fibers

## 1. Introduction

The scintillating tile detectors are the key elements of the Large Area Telescope (LAT) anti-coincidence detector (ACD), scheduled for launch early in 2008 as the main instrument of a new gamma-ray observatory, GLAST (Gamma ray Large Area Space Telescope). LAT [1] will detect celestial gamma-rays in the energy range from  $\sim 20 \text{ MeV}$  to  $> 300 \text{ GeV}$  with angular, energy, and time resolution substantially better than in its predecessor EGRET on the Compton Gamma Ray Observatory [2]. A detailed description of the ACD is given in Ref. [3], where most aspects of the system design, fabrication, and

tests are covered. The purpose of this paper is to provide the design and fabrication details for the ACD main component, the scintillator tile detector, and its readout.

The main purpose of the ACD is to detect charged particles efficiently and to create a veto signal that can be used to reject charged particles. The ACD is a square  $1.7 \text{ m} \times 1.7 \text{ m} \times 0.9 \text{ m}$  hat covering the top and four sides of the LAT (Fig. 1). The flux of charged particles in the GLAST orbit exceeds the flux of gamma-rays by 3–5 orders of magnitude, and the ACD has the primary responsibility for eliminating that charged particle background. This requires that the ACD efficiency for detecting singly charged relativistic particles (minimum ionizing particles (MIP)) be  $> 0.9997$ , averaged over its entire area of  $8.3 \text{ m}^2$ . The LAT is required to be sensitive to photons up to  $300 \text{ GeV}$  in the presence of backscatter from the electromagnetic showers created by the high-energy

\*Corresponding author. Tel.: +1 301 286 5581.

E-mail address: [Alexander.A.Moiseev@nasa.gov](mailto:Alexander.A.Moiseev@nasa.gov) (A.A. Moiseev).

<sup>1</sup>Retired.

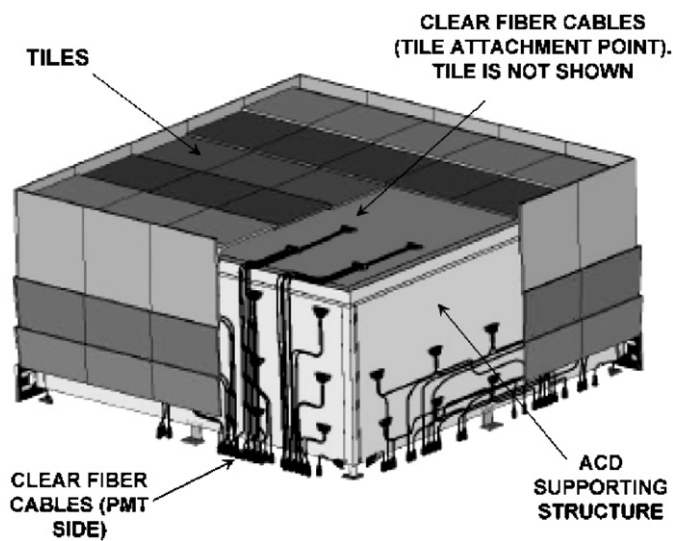


Fig. 1. ACD structure. The long tiles are not shown. PMTs (also not shown) are located around the bottom edge of the ACD.

gamma-rays in the LAT calorimeter. The higher the primary photon energy, the more intense the backslash is, so the approach is to “divide and conquer”. The ACD is segmented into an array of 89 separate tiles reducing the probability that the track (in the Tracker subsystem) points back to a scintillating tile with a signal from a backslash photon (see Refs. [3,4] for more details). The background particles are isotropic except for shadowing effects of the Earth and its magnetic field. In order to detect particles over all parts of the LAT field of view, we must minimize the “dead” areas, those without active detectors. These dead areas include the mechanical gaps between tiles created by the segmentation. These gaps are necessary in order to tolerate launch vibration and thermal expansion.

The requirement to have high detection efficiency for charged particles and at the same time low efficiency for backslash-caused signals in the ACD dictates careful optimization of the detection threshold. Therefore, it is critical that the detection threshold be highly uniform over the tile area. These requirements point to the need for high light output with good light collection uniformity over the tile area. An additional system requirement is to minimize the inert material in the instrument aperture, making it desirable to locate the light sensors remotely from the tiles.

Thus, the basic requirements for each tile detector can be summarized as follows:

- maximize light yield, providing average detection efficiency of  $>0.9997$  for a MIP;
- provide light production and collection uniform to  $\pm 10\%$  over the tile area;
- implement dual light readout to provide redundancy;
- provide robustness; and
- position the photomultiplier tubes (PMTs) to minimize inert material in the LAT field of view.

We describe, as follows, a design and its implementation that meet these requirements.

## 2. Tile detector design

### 2.1. Design overview

It was decided to use plastic scintillator for the ACD because it is the simplest, most reliable, and efficient in charged particle detection, nearly transparent to photons, well-understood, inexpensive, and robust detector technology; also, there was a great deal of experience with the material in space applications. The scintillator tile detectors are made of 1 cm thick polyvinyltoluene (PVT) plastic scintillator, ElJen-200, produced by ElJen Technology. (The five tiles in the top middle row are 1.2 cm thick, to compensate for the greater distance from the PMTs. We will discuss only 1 cm thick tiles in this paper.) The tile thickness choice resulted from a trade-off between minimizing mass (critical for space experiments) and maximizing light yield. The decisive step in the tile design was to choose the readout. The highest light yield could probably have been provided by direct PMT attachment to the scintillator, but the light collection uniformity requirement would have been hard to meet, and the PMTs would have been located in the LAT field of view. It was also unclear how to provide complete ACD coverage of the LAT field of view with such a readout. After a study of different design concepts, including optical light guides, wavelength-shifting (WLS) bars, directly coupled PIN photodiodes, etc., it was found that WLS fibers coupled to optical transmission fibers would be the best way to deliver the light to remotely located PMTs. This readout is widely used in accelerator experiments, with various modifications depending on the application (e.g. [5–10]). We used the heritage of those studies, but the specifics of a space experiment in general and the LAT requirements in particular demanded our own investigation and optimization of the detector.

We decided to build three basic shapes for the ACD tiles. In this paper, we will discuss these configurations: a rectangular “basic flat” tile 32 cm by various lengths (Fig. 2a); a “bent tile”, dimensioned to fill a 32 cm  $\times$  32 cm area after bending (Fig. 2b); and a rectangular “long” tile, 170 cm  $\times$  17 cm (Fig. 2c).

“Basic flat” tiles are the most numerous in the ACD design. Each tile has 64 keyhole-shaped grooves (see Section 2.3 for details) in which 1 mm diameter WLS fibers are embedded (Fig. 2a). Alternate fibers are gathered and routed to two different PMTs for redundancy. Details of the fiber layout are discussed in Section 2.3.

A “bent tile” covers the same area as a 32 cm  $\times$  32 cm “basic flat” tile, with the added complication that the scintillator has a 90° bend for use at two edges of the ACD top. These tiles cover the gaps where orthogonal tiles meet (see Fig. 1). The bend enables the fibers from top tiles to turn the corner to reach the PMTs. Special care was

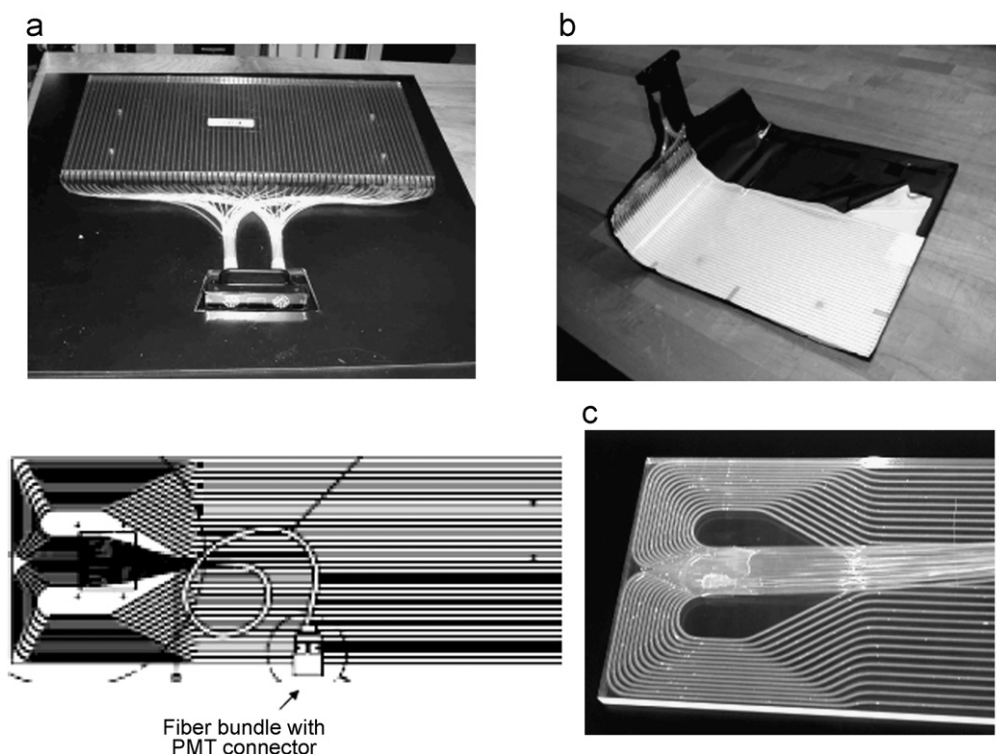


Fig. 2. (a) “Basic flat” tile, unwrapped. The fiber routing and optical connector are shown. (b) The “bent” tile with cutout to show the inner light-reflecting wrapping layers and the outer black light-tight layers. (c) The left half of a symmetrical “long” tile: left, drawing and right, photo of unwrapped tile.

required to bend the tiles properly; first, so as not to have the tile edges “bump out” at the bending line due to plastic deformation, and second, not to degrade the tile surface during thermal bending. We machined the tile edges after thermal bending to make the edges flat. The bending temperature was optimized at 65 °C so as not to degrade the scintillator performance (see more details in Section 3). Light collection uniformity was measured in the bent area and no significant degradation was found.

The “long” tiles, 170 cm long and 17 cm wide, are used around the bottom perimeter of the ACD. Due to the location of these tiles, the fibers must exit the tile surface as shown in Fig. 2c. This requirement creates an additional complexity in the fiber routing. To provide redundant readout, both sets of WLS fibers have to cover the whole tile. The 26 fibers are placed in curved grooves to collect light from the full tile area and are routed to exit the tile from its large surface. The fiber runs are comparable to the light attenuation length of the WLS fiber. Light attenuation in the tiles will be discussed in Section 4.

## 2.2. Approach to determining tile performance

For all measurements of scintillation light collection efficiency (light yield) and uniformity we used cosmic ray muons to measure the detector response. We express the light yield in units of the mean number of photoelectrons emitted from the PMT photocathode by the light produced by a single normally incident MIP in the scintillator.

To eliminate dependence on specific photomultiplier parameters (mainly photocathode quantum efficiency), the same physical PMT is used for all comparison measurements.

The approach to measuring the light yield is based on measuring the dependence of MIP detection efficiency upon the signal detection threshold. Fluctuations in the signal amplitude are determined by fluctuations in particle pathlength in the scintillator, ionization losses (Landau fluctuations), and statistical fluctuations in the number of photoelectrons. Measuring the detection efficiency for MIPs vs. detection threshold, expressed as a fraction of MIP peak position (on a PHA histogram), the light yield, or most probable number of photoelectrons, can be determined by fitting the efficiency dependence by a Poisson distribution with a given mean number. The typical position of the MIP peak on a PHA histogram (Landau distribution) is at ADC bin 400–500 (after pedestal subtraction), with FWHM of ~300 ADC bins. The experimental setup removed most pathlength fluctuations. This approach provides an “effective” light yield to characterize the detector efficiency, which is slightly less than the true efficiency.

The experimental setup for this measurement is shown in Fig. 3, where the light yield is measured for the “Tested Tile”. Since we want to measure the detection efficiency with high accuracy, a clean sample of quasi-vertically incident muons passing through the central portion of the tile is selected by means of four-fold coincidence of signals



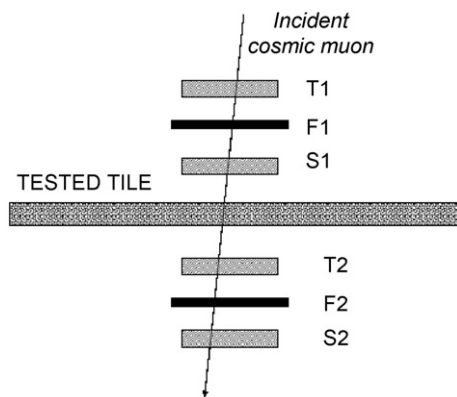


Fig. 3. Experimental setup for the efficiency measurement with cosmic muons. The muons are selected by four-fold coincidence of the signals from S1, S2, T1, and T2 scintillators. Lead filters F1 and F2 are used to remove the electron component.

from triggering scintillators S1, S2, T1, and T2 (all 5 cm × 5 cm). Two 5 mm thick lead filters, F1 and F2, are used to remove electrons, and signals from T1 and T2 are required to be within the amplitude range 0.3–1.8 of the most likely pulse height. This selects muons. An example measurement result is shown in Fig. 4, where the experimental data are fitted by Poisson distributions corresponding to two different mean values.

The “long” tile has relaxed requirements for light yield and light collection uniformity; its MIP detection efficiency must be >0.99. Because light attenuation in the long WLS fibers is important for the “long” tile, with fiber length comparable to the WLS fiber attenuation length, we measured the MIP detection efficiency and light yield at three points along the tile length, in the center and near the ends (see Section 4 for details).

As mentioned above, each tile must have uniform light collection over its area. In the design phase, we measured the uniformity by using two plastic scintillating hodoscopes specially designed and built for these tests. This technique provided coarse mapping of the tile light yield with 4 cm × 4 cm pixels. After the ACD integration in the LAT, the tile light collection uniformity was measured on a finer spatial scale with the help of the LAT Tracker, which reconstructed the position of the particle in the tile with a precision of better than 1 mm. With these measurements, we determined that the light collection uniformity is within ±5% over the tile area except in a ~2 cm border area, where the light output gradually degrades to ~80% of its value at the tile center.

### 2.3. Tile design optimization

As mentioned above, WLS fibers, embedded and glued in grooves, collect the light from all three types of tile detectors. This technique, while not the best from the point of view of the amount of light collected, provides the best light collection uniformity over the tile area and allows remote positioning of the PMT.

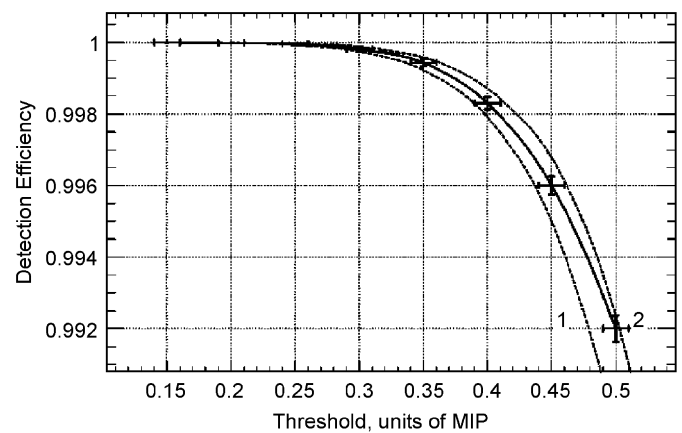


Fig. 4. Measured detection efficiency (the solid line through the data points is shown to guide the eye.) vs. signal detection threshold, expressed in units of MIP fraction. Computed Poisson distributions for mean photoelectron numbers of 20 (dashed line 1) and 22 (dashed line 2) photoelectrons are shown to determine the light yield of the tested tile.

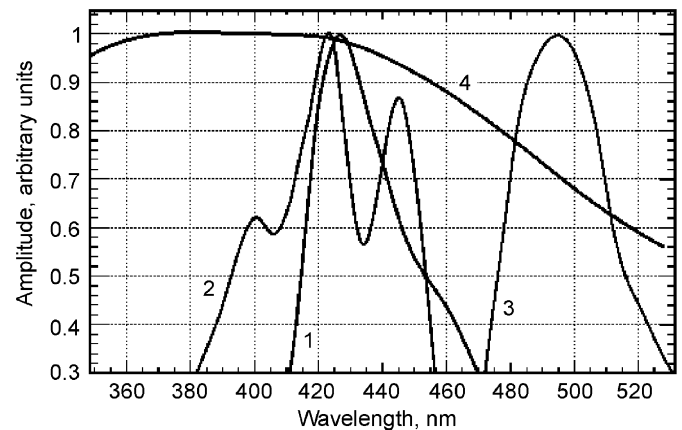


Fig. 5. Optical spectra: line 1, emission spectrum for EJ200 scintillator; lines 2 and 3, respectively, absorption and emission spectra for WLS fiber BCF-91A; and line 4, scaled to its maximum value quantum efficiency for Hamamatsu R-4443 PMT.

In order to optimize the light collection in the approach used, the absorption spectrum of the WLS should match the emitting spectrum of the scintillator. The EJ200 scintillation light emission peak is at 425 nm and is a good match to the BCF-91A maximum absorption wavelength range (410–460 nm), providing maximal light conversion for transmission to the PMT (Fig. 5). We also investigated the effect of fiber cladding. It was found that the use of multicladd fibers increased the light yield by 20–25%. For gluing fibers into grooves, we used optical epoxy BC-600 (made by Saint-Gobain) as the best match to our scintillator. The CMS experiment [5] also used scintillating tiles with WLS fiber readout, but did not bond the fibers; they were simply inserted into keyhole-shaped grooves (Fig. 6). We found that bonding the fibers gives at least a factor of 2 increase in light, which was critical for our application but was not so important in CMS tiles, where

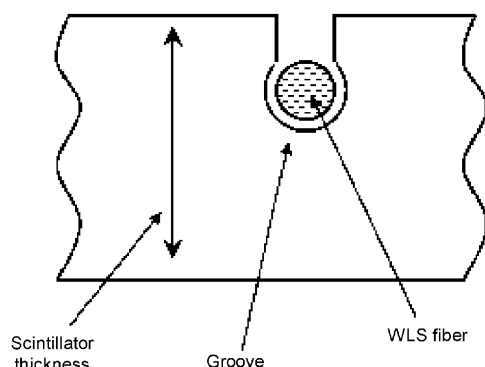


Fig. 6. Keyhole-shaped groove.

the cost of mass production of thousands of tiles was the driver.

The choice of PMT proved to be important in optimizing the light detection. First, the quantum efficiency varies significantly even within same type of PMT, so PMT selection helps greatly. The use of “green” WLS fibers is not a good match to the efficiency of a conventional bialkali photocathode (maximum response at  $\sim 420$  nm), because it reduces quantum efficiency at the 490 nm emission peak of BCF-91A (Fig. 5). One possibility was to use PMTs with a green-extended photocathode. However, we found that the Hamamatsu R4443 (which was chosen for the project), a ruggedized version of conventional Hamamatsu R647, could not be manufactured in a ruggedized version with green-extended photocathode. We, therefore, decided to select normal bialkali PMTs for maximum quantum efficiency at 490 nm. It appeared that most of the selected tubes were not the best performers at the nominal 420 nm wavelength but had flatter dependence of quantum efficiency upon wavelength and thus had better quantum efficiency at 490 nm. In the end, the PMTs selected for the project had quantum efficiencies in the range 18–25% at 490 nm.

An optimization study on the depth and spacing of the grooves in the scintillator was performed (Table 1). It was found that embedding the fibers 2 mm deep and with 5 mm spacing between grooves gave the best results. Use of two PMTs is dictated by the space experiment reliability requirements, to provide redundancy in case of PMT failure. We found that routing alternate fibers to the two different PMTs was optimal.

We studied other design options, such as not embedding the fibers into the scintillator but bonding them directly to the surface of the tile continuously (without gaps between fibers), or to the edge of the tile. The former design, in spite of demonstrating high performance, was rejected due to requiring too many fibers (number of fibers was restricted by the PMT photocathode area). The latter design demonstrated significant decrease in light collection efficiency (about 50%). We also considered other “winding” patterns of grooves in the scintillator that would simplify the fiber bundling and routing outside the tile, but found

Table 1  
Light yield vs. spacing of WLS fibers

Fiber spacing (cm)	Light yield (arbitrary units)
2	15.9
1	18.1
0.5	22.0
0.25	20.2
Continuous	23.3

them to be impractical due to more complicated and expensive groove machining and fiber population.

Embedding the fibers in keyhole-shaped grooves [5] provides convenience and confidence in securely holding the fibers in the grooves. It proved to be especially important in the bent tiles, where the fibers could easily escape from the grooves in the bending zone if they were not secured by the key shape of the grooves. In order to protect the fibers against cracking at the exit point from the tiles, thin flexible tubing about 2 cm long was placed over each fiber.

If the fibers are read out from one end (as in “basic flat” and “bent” tiles), the treatment of the unused end is important to return some portion of the light to the collection end. We found that aluminizing the end yielded  $\sim 20\%$  higher light collection in comparison with only polished fiber ends, so all open fiber ends were aluminized (see Section 3 for details).

#### 2.4. Tile detector packaging

In accordance with the requirement of minimal inert material in the sensitive area, each tile is not boxed or framed but rather is enclosed within a light-tight wrapping. This constraint created substantial problems in finding the proper materials and establishing the wrapping procedure. The inner wrapping layer must provide good light reflection, and the outer layer must provide light tightness (see Fig. 2b). It is important to have the surfaces of the scintillator polished so that they reflect at least 50% of the scintillation light inside the scintillator. The inner wrapping, in turn, has to maximize the return of escaping light to the scintillator. We studied three different wrapping materials: Tyvek, Tetratex, and Polyester (choice limited by materials permitted for use in space experiments). We found that the best results can be achieved with two layers of 0.25 mm thick Tetratex (a Teflon-based material).

Light from external sources (sunlight in particular) must be prevented from entering the tiles. The external wrapping, providing light tightness, is two layers of 50  $\mu$ m thick black Tedlar. Light tightness measurements that we made demonstrated that the two layer wrapping absorbs all incident light, with any remaining light leak limited by the measurement technique sensitivity, corresponding to the signal from less than 0.5 photoelectron.

Because the tile detectors must operate in vacuum, proper venting of the tile envelope must be provided.

This requirement created additional difficulty due to conflicts with the light tightness requirement. In order to provide the venting, the process of wrapping with overlapping layers was carefully designed. A fraction of the seams in the outermost wrapping layer were left partially untaped to allow venting to take place.

Since the tile design is “frameless”, the tile mounting was an issue. It had to take into account the required minimization of dead areas, or gaps, between adjacent tiles. The final design has every tile mounted to the ACD structure by four 3 mm diameter screws that go through the scintillator. The “long” tiles have 14 screws. The holes are drilled between the fibers, with special care not to have the response distorted in the vicinity. We investigated whether the scintillator can be damaged by the screws during mechanical vibration and found no performance degradation after those tests. The effect of the dead area caused by the holes was studied and determined to cause degradation in detection efficiency for an isotropic incident flux of less than 0.00005. Light sealing in the vicinity of the screws was provided by the use of special black rubber washers.

### 2.5. Light transport from the tiles to the PMTs

The design of ACD, with the PMTs located around the base of the ACD (outside the LAT field of view), results in different distances between the tiles and the PMTs, up to about 1.5 m. We considered two approaches to delivering the light from the tile to PMT. The first option was to run WLS fibers all the way, and the second was to mate the WLS fibers to clear optical fibers or “cables”. We measured the attenuation length of WLS fibers to be  $\sim 1.6$  m, slightly changing along the fiber according to the distance from the tile. The attenuation length for clear fibers was measured to be  $\sim 6$  m. Both these numbers were obtained for our relatively short fiber runs and can be larger for longer fiber lengths. To maximize the amount of scintillating light delivered from the scintillator to the PMT, the optimal design uses the first option for the tiles with total fiber runs less than 40 cm, and the second option for longer fiber runs. For the clear fiber cables, 1.2 mm diameter BC-98 fibers (from Saint-Gobain) are used. The larger diameter (WLS fibers are 1 mm diameter) allows for tolerance in fiber mating alignment.

We investigated two options for fiber mating: (1) optical mating in specially designed connectors and (2) thermal coupling as used in CMS [5,11]. No grease was allowed due to the space flight requirements. For our detector, we chose the former method to permit for easy de-mate and re-mate if needed, to simplify ACD integration and servicing. No significant difference was found in the light conduction efficiency between these two options, both of which suffer 15–20% light loss at the point of fiber mating.

One issue that arose was how to bundle the fibers at the output from the tile and provide light tightness at the point where the fiber bundle split in two for the two redundant



Fig. 7. Optical fiber-to-fiber mating connector. Alignment pins are seen on the right (clear fiber) side. Opaque tubing that surrounds the fiber bundles has been removed for clarity.

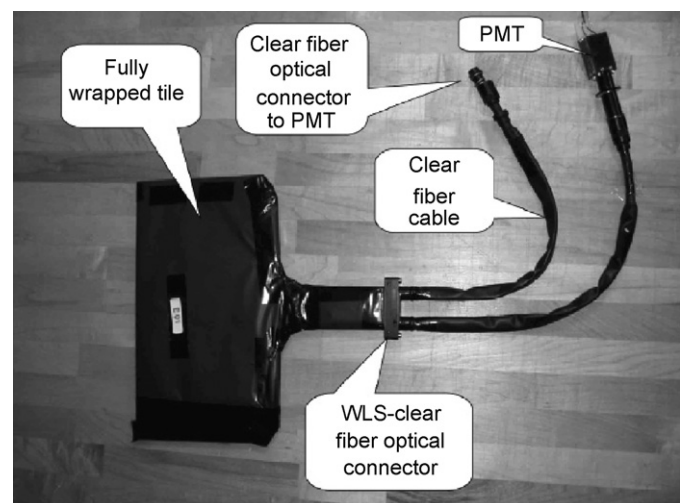


Fig. 8. Assembled “basic flat” tile.

PMTs. A special interface was designed with two versions. An optical connector (Fig. 7; also seen in Fig. 2) does fiber mating and consequently requires precise machining to provide fiber alignment and fiber end polishing to provide the best light conduction. A pass-through connector (for those tiles where the light is delivered by only WLS fibers) is needed only to provide light tightness in the transition point from the tile to the fiber bundles. Its design is similar to that of the mating connector, but it consists of only one pass-through part. Both those connector types split the fibers from a tile into two bundles, to be routed to different PMTs, and provide venting as well. Fiber bundles and clear fiber cables are inserted in Sumitube black tubing (made by Sumitomo Electric). The tubing provides light tightness and connects to the PMT housing. Fig. 8 shows the whole tile-to-PMT assembly.



### 3. Tile fabrication

Fabrication of the tiles is a critical step in achieving high performance and implementing all findings of the design studies. The intended 10-year lifetime in space requires that a clean environment be maintained during tile fabrication, to prevent scintillator crazing from foreign residuals (e.g. human and mechanical oil). Prototyping and fabrication of the tiles was performed at Fermi National Accelerator Laboratory (FNAL). In this section, we describe the main steps in tile fabrication.

#### 3.1. Plastic scintillator sheet inspection and preparation

Initial inspection of the scintillator was performed in order to find any obvious damage or flaws, before any operations were performed. Special care was taken to check the scintillator sheet flatness and thickness uniformity, both to be within 0.15 mm. (In order to meet these rather tight flatness and thickness uniformity requirements, EJen cast the scintillator in pieces that were considerably smaller than their normal castings.) Final scintillator quality inspection was performed when the scintillator was unwrapped for cutting to size. Rubber gloves were mandatory during the handling of unprotected scintillator. No scratches or scintillator damage were allowed. At this point, each tile was assigned an ID number and traveler, used as an aid in the assembly steps. Each step was signed off by the technician who performed the step, as well as a Quality Assurance representative.

#### 3.2. Groove cutting

This operation is critical for maximizing light collection. Proper tools and optimized cutting speed are the decisive factors. An improper tool or cutting speed can cause optical defects, in particular scintillator melting, which is essentially impossible to remove. The tiles were first cut to size, and the edges were diamond-polished. After the mounting holes were drilled, grooves were cut by an Axxiom CNC according to files programmed for each tile configuration. Special care was taken to cool the cutting area, using cold air, to prevent scintillator melting (Fig. 9). The Axxiom tool speeds were adjusted daily, depending on temperature and humidity. Test cuts were performed to assure the cuts were clean and the tool speeds were adjusted for optimizing the quality of the cuts. Several passes were performed for each groove, to improve the quality of the cuts and allow the best transmission of the scintillating light through the cut surfaces.

After completion of groove cutting, the tiles are annealed at 70 °C for 3 h. This removes any remaining stress in the scintillator, which can cause crazing and consequent performance degradation.



Fig. 9. Tile groove cutting.

#### 3.3. Tile bending

This operation was performed to create the “bent” tiles. The Tile Forming Fixture was cleaned and preheated before each use. The tile bending edge is preheated to 65 °C and maintained throughout the forming process. The tile was placed in a preheating fixture and heated for approximately 10 min, then removed from the fixture and placed on the forming fixture. A forming sheet was placed over the tile, forcing it to conform to the fixture. Weights were added and the fixture and tile were allowed to return to ambient room temperature. Once cooled, the tile was inspected for any crazing or damage from the process.

#### 3.4. Fiber preparation and gluing

Wavelength-shifting fibers are the key element in the tile detector, and tile light yield critically depends upon their performance. Fibers with damaged outer cladding, which can be found visually by characteristic bright rings, were removed during the initial fiber inspection. The next step was to mirror the fiber ends. The fiber ends were first ice-polished (polished in a frozen state), then sputtered with aluminum and finally coated with a protecting chemical and cured for 15 min with UV lamps. This process secures the best internal reflection and long time stability.

#### 3.5. Gluing the fibers into the grooves

Special care must be given to eliminate air bubbles in the glue, which dramatically reduce the collected light. Prior to gluing the fibers into the grooves, the entire tile surface was temporarily covered by 3M8901 tape to prevent the glue from spilling out of the grooves and degrading the internal reflection performance of the tile surface. The BC-600 optical epoxy was mixed and then set into a vacuum chamber for several minutes to remove air bubbles from the mixture. The mixture was then transferred to an



injection applicator and injected into the fiber grooves. Injecting the mixture slowly was important, to allow for time for the air in the groove to vent and be pushed out. Slight movement of the fiber was sometimes needed to help loosen the trapped air inside the groove and allow it to be pushed out.

### 3.6. Optical connector installation

Fibers were routed to the connectors, alternating every other fiber to one of the two connector outlets (Figs. 7 and 10). The demanding requirement in fiber routing was that the dimension “ $d$ ” in Fig. 10 (lower panel) was limited, in some cases to as little as 23 mm, due to ACD mechanical constraints. Taking into account that the allowed minimum fiber bending radius is 20–25 mm, this represented a challenge. In order to achieve this, a special routing template was made, different for each tile type (Fig. 10, upper panel). Use of these templates assured that the fiber length from tile to connector was correct, the fibers were all relaxed and that no fiber was tighter than the others. Once the fibers were in place, they were taped to the template to prevent movement. The next step was inserting the fibers in

the connector holes (also ordered to minimize fiber crossing) and filling the holes with BC-600 glue, using a syringe.

After the BC-600 glue was cured, the routing template with the tile and connector was annealed for 3 h at 70 °C, followed by return to room temperature over a 12 h interval. Fiber stresses were relieved by this operation. Finally, polishing was performed on the fiber/connector ends, by freezing the fiber ends, then polishing them with an ultra high-speed diamond cutter. After polishing, each batch was inspected under magnification for any damage or smudges to assure that the surfaces met specifications. A tile is shown in Fig. 2a after completion of this step.

### 3.7. Tile wrapping

The final operation in tile production was wrapping. As described in Section 2.4, the wrapping includes two inner light-reflecting layers of white Tetratex, and two outer light-tight layers of black Tedlar. After wrapping, the tile was subjected to a light tightness test, performed by connecting a PMT to the optical connectors and comparing the signal rate (with discriminator threshold set to  $\sim 0.5$  photoelectron) with the tile covered by a light-tight blanket and without it. The tile was considered to be light tight if the difference was less than the statistical error in the rate measurement.

## 4. Discussion of the tile detector performance

As a result of numerous optimization studies, the light yield performance of 85 tile detectors of different sizes and shapes (excluding the long tiles), is shown in Fig. 11 (each tile shown twice because of two PMTs), with a mean value of  $\sim 20$  photoelectrons. These results were obtained from a setup with a fiber mating optical connector and with  $\sim 20$  cm long clear fiber cable extension. We estimate that in this setup, the WLS fiber bundle, the connector and clear fiber cable acting together reduce the light by  $\sim 30\%$  with

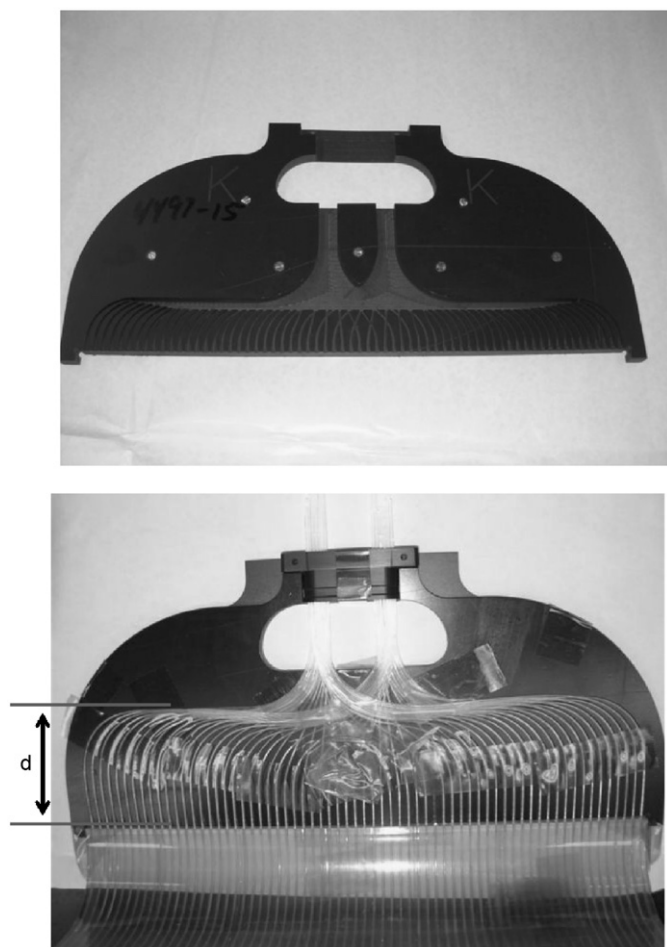


Fig. 10. Fiber routing. Upper panel—routing template; lower panel—fibers routed on the template.

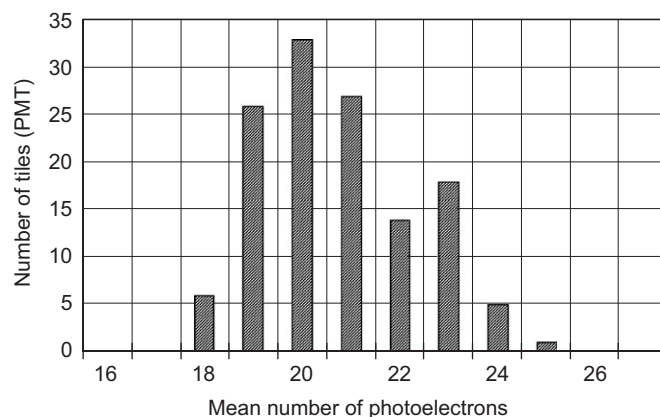


Fig. 11. Distribution of the measured photoelectron yield for 170 ACD tile channels (“long” tiles excluded; two signals from each remaining tile; two PMTs per tile).

respect to that coming out of the tile. Essentially no difference was found in performance between the “basic flat” and “bent” tiles. It is important to note that Fig. 11 shows the light yield after splitting the light between two PMTs, so it would approximately double if the tile fibers were viewed by a single PMT. A tile with two PMTs operating in “OR” demonstrates muon detection efficiency of  $>0.9999$  with the detection threshold set to 0.3 MIP, and  $>0.9990$  in case of failure of one PMT (results obtained with cosmic muons as described in Section 2.2). Taking into account attenuation in the fiber cable and light splitting to two PMTs, we estimate that the light yield for our tile detectors would be  $\sim 60$  photoelectrons if they were read out by a single PMT without the optical fiber coupling. All of these measurements were made with the same relatively poor “testing” (non-flight) PMT with quantum efficiency of  $\sim 15\%$  at 490 nm. The flight ACD utilizes PMTs selected for quantum efficiency  $>19\%$ , which raises our estimate of single tile light yield to  $\sim 75$  photoelectrons.

The tile detector design was also tested in accelerator beams [4,12,13] and in a balloon flight [14], confirming the performance measurements and demonstrating high reliability and easy handling. It is not easy to compare our results directly with those reported by other groups because the performance is strongly affected by the application-driven detector designs. Various authors report light yields for MIPs achieved by different plastic scintillator detectors with WLS fiber readout, ranging from a few to about 100 photoelectrons per centimeter of scintillator thickness [5–10]. Our detectors are therefore among the best.

Fig. 12 shows the light output profile, across the fibers, for a tile, obtained with a relativistic carbon beam [13]. The data were taken using the “high” range of ACD electronics, which allows us to register high amplitude signals from heavy cosmic ray nuclei. The signal for carbon is  $\sim 700$ – $800$  photoelectrons so the tile energy resolution is

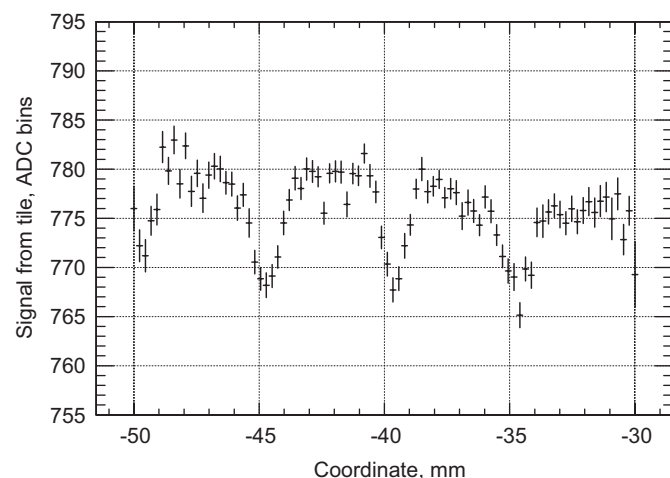


Fig. 12. Signal profile for the central part of a tile (across the fibers) obtained with a carbon beam. The dips separated by  $\sim 5$  mm correspond to the fiber pitch, resulting from thinning of the tile by the fiber groove depth.

determined only by the ionization losses fluctuation and reaches a value of  $\sim 15\%$  FWHM. This energy resolution makes it possible to see the effect of the WLS fibers (“dead” material) embedded in the tile; the fiber pitch is 5 mm.

Light yield for a “long” tile is shown in Fig. 13 (upper panel) for a PMT viewing the tile from one end, as a function of the muon impact coordinate. The PMT on the opposite end has similar performance. Fig. 13 (lower panel) shows the resulting normal incidence MIP detection efficiency vs. the muon traversal coordinate along the tile with detection threshold set to 0.3 of a MIP mean value. The flat line representing the sum signal does not fall below 0.9998, demonstrating high and uniform detection efficiency for such a long scintillator paddle. It is also seen that for only one PMT, the MIP detection efficiency is  $>0.98$  over the entire detector area.

In order to assure that the assembled flight tile detectors meet the requirements for use in a space flight experiment, a number of environmental and mechanical tests were performed successfully. We briefly mention here the tests which are essential. Vibration tests included random vibrations along three axes, from 20 to 2000 Hz, and sine burst normal to the tile plane. After each axis vibration, the total light yield and light yield mapping (with  $4\text{ cm} \times 4\text{ cm}$  pixels; see Section 2.2 for details) were measured. Light yield mapping was needed to reveal possible damages in fiber gluing, which would affect the light yield from a particular tile area. No detectable degradation was observed. A thermal cycling test was performed to assure that there will be no defects or cracks in the fibers themselves, or their gluing, due to the thermal stress. No significant light yield change was found after 440 cycles

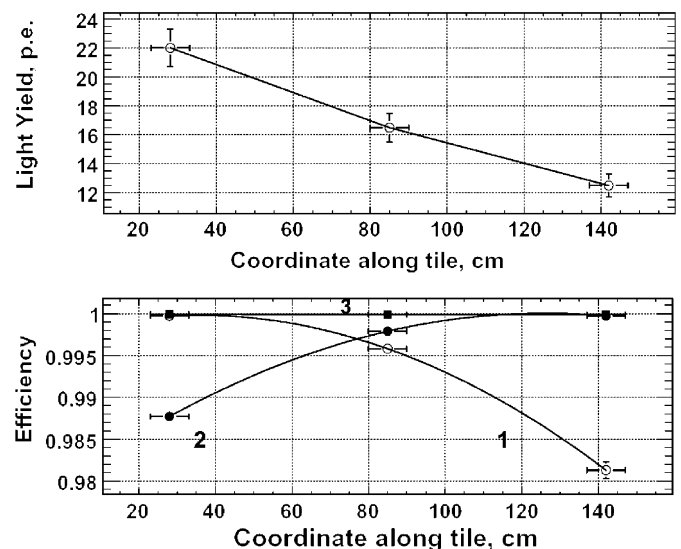


Fig. 13. Performance of the “long” tile: the upper panel shows the light yield obtained at one end of the tile vs. the distance along the tile to the muon traversal point. The bottom panel shows the efficiency of muon detection vs. the muon traversal point for the PMT at the “0 cm” end (line 1, open circles), at the opposite end (line 2, filled circles), and for both PMT operating together (line 3, filled squares).

over the temperature range from  $-60$  to  $+45^{\circ}\text{C}$ . A vacuum test was performed in order to determine possible damage to the light-tight envelope during the rapid pumpdown from normal atmospheric pressure to vacuum. No light leaks were observed after 10 cycles.

## 5. Conclusions

We designed, fabricated, and investigated the performance of scintillator tile detectors with WLS fiber readout of various sizes (from  $450$  to  $2500\text{ cm}^2$ ) and shapes (flat and bent). Intended for use in the space gamma-ray observatory GLAST, the detectors meet all the requirements for a space experiment and are optimized to have maximum light yield combined with highly uniform spatial response. The tiles are read out using variable lengths of flexible light-transmitting cable, made of clear fibers that are mated to the tile WLS fibers by custom-designed optical connectors. This allows the use of remotely positioned PMTs outside the active area of the LAT instrument. Such a design would be useful in an experimental setup where the PMT cannot be placed next to the detector due to integration constraints or magnetic field issues. Each tile is read out by two PMTs that operate simultaneously in an “OR” mode, achieving  $>0.9999$  MIP detection efficiency. Were redundant readout not required, the scheme presented here could be easily modified for a single PMT, doubling the number of collected photoelectrons in a single PMT. We achieved an average effective light yield of  $\sim 20$  photoelectron for dual readout with optical connectors and  $\sim 20\text{ cm}$  long clear fiber cables. In the case of single PMT readout with optimized optical transmission and carefully selected PMTs, the light yield could reach at least 75 photoelectrons. The light collection is uniform over each tile area and is well within  $\pm 5\%$  of its mean value, with some decrease at the tile edges.

## Acknowledgments

The authors express their gratitude to Eileen Hahn, John Korienek, Jon Blomquist, and others from FNAL for their excellent work on the tile detector fabrication, and Pawel de Barbaro, also from FNAL, for valuable suggestions on the tile design. We thank ACD technicians at NASA

Goddard Space Flight Center (Deneen Ferro, Bill Daniels, Nick Kwiatkowski, Tom Huber) and the entire LAT ACD team for their critical contributions in all steps of tile detector design, fabrication, and testing. We are grateful to the Hamamatsu group, and especially Andrew Allen and Yuji Yoshizawa, for providing excellent phototubes that were specifically tailored to meet our goals. Support and suggestions from LAT team members and the members of LAT Calibration and Analysis group in particular, are greatly appreciated. We especially thank our LAT internal reviewers Gary Godfrey and Mario Nicola Mazziotta for careful reading of the manuscript and valuable comments and suggestions.

## References

- [1] W.B. Atwood, et al., *ApJ*, being submitted (2008).
- [2] E.B. Hughes, R.J. Hofstadter, A. Johansson, D.L. Bertsch, W.J. Cruickshank, C.H. Ehrmann, et al., *IEEE Trans. Nucl. Sci.* NS-27 (1980) 364;
- [3] C.E. Fichtel, *Astron. Astrophys. Suppl.* 120 (1996) 23.
- [4] A.A. Moiseev, R.C. Hartman, J.F. Ormes, D.J. Thompson, M.J. Amato, T.E. Johnson, et al., *Astropart. Phys.* 27 (2007) 339.
- [5] A.A. Moiseev, J.F. Ormes, R.C. Hartman, T.E. Johnson, J.W. Mitchell, D.J. Thompson, *Astropart. Phys.* 22 (2004) 275.
- [6] S. Aota, T. Asakawa, K. Hara, E. Hayashi, S. Kim, K. Kondo, et al., *Nucl. Instr. and Meth. A* 352 (1995) 557.
- [7] A.P. Ivashkin, Yu.G. Kudenko, O.V. Mineev, J. Imazato, *Nucl. Instr. and Meth. A* 394 (1997) 321.
- [8] O. Mineev, E. Garber, J. Frank, A. Ivashkin, S. Kettell, M. Khabibullin, et al., *Nucl. Instr. and Meth. A* 494 (2002) 362.
- [9] M. Beddo, E. Bielick, T. Fornek, V. Guarino, D. Hill, K. Krueger, et al., *Nucl. Instr. and Meth. A* 499 (2003) 725.
- [10] M.V. Diwan, *Nucl. Phys. B (Proc. Suppl.)* 123 (2003) 272.
- [11] S. Kuhlmann, H. Frisch, M. Cordelli, J. Huston, R. Miller, S. Lami, et al., *Nucl. Instr. and Meth. A* 518 (2004) 39.
- [12] K. Hara, K. Horiuchi, S. Kim, I. Nakano, T. Takebayashi, K. Takikawa, et al., *Nucl. Instr. and Meth. A* 348 (1994) 139.
- [13] W.B. Atwood, S. Ritz, P. Anthony, E.D. Bloom, P.E. Bosted, J. Bourotte, et al., *Nucl. Instr. and Meth. A* 446 (2000) 444; E. do Couto e Silva, P. Anthony, R. Arnold, H. Arrighi, E. Bloom, B. Baughman, et al., *Nucl. Instr. and Meth. A* 474 (2001) 19.
- [14] L. Baldini, G. Barbiellini, R. Bellazzini, J.R. Bogart, G. Bogaert, E. Bonamente, et al., in: S. Ritz, P. Michelson, C. Meegan (Eds.), *Proceedings of the First GLAST Symposium*, AIP 921, 2007, p. 190.
- [15] D.J. Thompson, G. Godfrey, S.M. Williams, J.E. Grove, T. Mizuno, H.F.-W. Sadrozinski, et al., *IEEE Trans. Nucl. Sci.* NS-49 (4) (2002) 1898.